Thermal convection in a thermosensitive colloidal suspension

New Journal of Physics
The open access journal at the forefront of physics
Deutsche Physikalische Gesellschaft DPG | IOP Institute of Physics

Corrigendum: Thermal convection in a thermosensitive colloidal suspension (2010 *New J. Phys.* **12** 053003)

Florian Winkel[1,3], Stephan Messlinger[1], Wolfgang Schöpf[1], Ingo Rehberg[1], Miriam Siebenbürger[2] and Matthias Ballauff[2,4]

[1] Experimentalphysik V, Universität Bayreuth, D-95440 Bayreuth, Germany
[2] Physikalische Chemie I, Universität Bayreuth, D-95440 Bayreuth, Germany
E-mail: ingo.rehberg@uni-bayreuth.de and matthias.ballauff@helmholtz-berlin.de

New Journal of Physics **16** (2014) 079501
doi:10.1088/1367-2630/16/7/079501

We found two errors in the paper 'Thermal convection in a thermosensitive colloidal suspension' (2010 *New J. Phys.* **12** 053003), which were both originally our mistake.

In table 1, two units are wrong. The solutal expansion β has no unit, while the unit of the Soret coefficient S_T is 1/K. The respective lines in this table should correctly read:

Solutal expansion	β		0.0938 ± 0.0004	—
Soret coefficient	(S_T)	(K^{-1})	0.35 ± 0.03	—

[3] Current address: Max-Planck-Institute for Dynamics and Self-Organization, Bunsenstrasse 10, D-37073 Göttingen, Germany.
[4] Current address: Institut für Physik, Humboldt–Universität zu Berlin, Unter den Linden 6, D-10099 Berlin, Germany.

New Journal of Physics
The open-access journal for physics

Thermal convection in a thermosensitive colloidal suspension

Florian Winkel[1,3], **Stephan Messlinger**[1], **Wolfgang Schöpf**[1], **Ingo Rehberg**[1,5], **Miriam Siebenbürger**[2] **and Matthias Ballauff**[2,4,5]

[1] Experimentalphysik V, Universität Bayreuth, 95440 Bayreuth, Germany
[2] Physikalische Chemie I, Universität Bayreuth, 95440 Bayreuth, Germany
E-mail: ingo.rehberg@uni-bayreuth.de and
matthias.ballauff@helmholtz-berlin.de

New Journal of Physics **12** (2010) 053003 (18pp)
Received 18 December 2009
Published 5 May 2010
Online at http://www.njp.org/
doi:10.1088/1367-2630/12/5/053003

Abstract. Thermal convection is investigated experimentally in a microgel suspension that consists of core-shell colloids, which change their size with temperature. The swelling and shrinking of the particles strongly modify their volume fraction in the carrier fluid and therefore the viscosity of the suspension. In this experiment, thermal convection in a Hele–Shaw-like apparatus is monitored using the shadowgraph technique. When compared to a normal fluid, the threshold temperature difference is reduced dramatically, which is interpreted as a manifestation of the Soret effect, i.e. the temperature gradient applied to the suspension induces an unstable gradient of the colloid concentration. The wavelength in the nonlinear regime is very different from the one observed in water. Furthermore, transient oscillations of the patterns are detected in the nonlinear regime and are investigated as a function of the applied temperature difference.

[3] Current address: Max-Planck-Institute for Dynamics and Self-Organization, Bunsenstrasse 10, 37073 Göttingen, Germany.
[4] Current address: Institut für Physik, Humboldt–Universität zu Berlin, Unter den Linden 6, 10099 Berlin, Germany.
[5] Authors to whom any correspondence should be addressed.

Contents

1. Introduction

Colloidal suspensions, such as wall paint, ice cream or sunscreen, cover a wide range of substances, not only in an industrial but also in our everyday life environment [1]–[3]. Their significance further extends to a variety of biological systems, such as suspensions of algae in water, single-cell bacteria or the bloodstream in human bodies. One prominent effect in colloidal suspensions is thermal diffusion (or the Ludwig–Soret effect), which leads to a partial separation of the components caused by thermal gradients [4, 5]. This might have played some role in the formation of life in the so-called 'hydrothermal vents' or 'black smokers' [6, 7].

The Ludwig–Soret effect influences another important temperature-driven hydrodynamic effect, namely thermal convection [8, 9]. Here, a macroscopic current is observed when a fluid layer between two parallel horizontal plates is heated from below and when the applied temperature difference ΔT exceeds a certain critical threshold value. This happens when the destabilizing buoyancy force overcomes the stabilizing dissipative force. The ratio of the counteracting forces can be expressed as a dimensionless control parameter describing the instability, namely the Rayleigh number

$$R = \frac{\alpha g d^3}{\kappa \nu} \Delta T. \tag{1}$$

Here, α is the thermal expansion coefficient, g the acceleration due to gravity, ν the kinematic viscosity, κ the thermal diffusivity and d the distance between the plates.

In its simplest case, the Rayleigh–Bénard convection in a pure single-component fluid, straight parallel convection rolls can be observed at threshold. The instability occurs for critical values $R_c = 1708$ of the Rayleigh number and $\lambda_c = 2.016\,d$ of the wavelength, both being independent of the material characteristics of the special fluid under consideration. Due to its simplicity, which nevertheless leads to a large variety of patterns and selection mechanisms

above the convection threshold, this system has been studied in great detail experimentally and theoretically in the linear (i.e. near threshold) as well as in the nonlinear (far from threshold) regime [8], [10]–[13].

If the convecting fluid consists of a mixture of two components (a *binary mixture*), the concentration of the components may strongly influence the bifurcation behaviour [14, 15]. Due to the Soret effect, the concentration field is coupled to the temperature field. The strength of the coupling is described by the Soret coefficient S_T, resulting in a second control parameter, namely the separation ratio

$$\Psi = \frac{\beta}{\alpha} S_T c(1-c), \tag{2}$$

where β is the expansion coefficient due to concentration changes and c is the concentration of the denser component. S_T (and thus Ψ) can have either sign and may have a stabilizing or a destabilizing effect on the conductive state. For $S_T > 0$, the Soret generated concentration current enhances the thermally induced density gradient, so that convection sets in for a lower Rayleigh number compared to a normal fluid (positive Soret effect). For $S_T < 0$, on the other hand, the thermally induced density gradient is diminished and convection sets in for a higher Rayleigh number (negative Soret effect). The dynamics of the concentration is driven by an independent time scale caused by the mass diffusivity D and expressed by the Lewis number $L = D/\kappa$. Hence, the time constant for the development of thermal convection is determined by the mass diffusion time $\tau_D = d^2/(\pi^2 D)$, which is typically much larger (by a factor of $1/L$) than the thermal diffusion time. For certain fluid parameters, this may lead to temporal oscillations at the convection threshold, which, combined with the spatial periodicity of the pattern, results in travelling waves for negative Ψ. Rayleigh–Bénard convection in binary mixtures, such as salt water, water–alcohol or ^{3}He–^{4}He, is readily accessible to high-precision experiments and thus a vast amount of literature is available [12], [14]–[17].

If the material parameters are such that $\Psi/L \gg 1$ (as it is the case in our experiment, see later), the Soret-driven convection sets in at an (analytically exact) critical Rayleigh number of $R_c = 720\,L/\Psi$ with an infinite wavelength of $\lambda_c = \infty$ [18]–[21]. Therefore, the appropriate control parameter for this case is the solutal Rayleigh number

$$R_s = R\frac{\Psi}{L} = \frac{\beta g d^3}{D\nu}\Delta c \tag{3}$$

with a concentration difference $\Delta c = S_T c(1-c)\Delta T$ between top and bottom boundaries and a critical value of $R_{s,c} = 720$. Compared to equation (1), the thermal properties of the liquid have been replaced by the corresponding solutal properties.

Although the current mathematical formalism for convection in binary molecular mixtures and for convection in colloidal suspensions is identical, the Soret-driven mass current in the latter case is often called *thermophoresis* instead of *thermal diffusion*. The large size of the particles ($\approx$1 nm–1 μm) leads to even longer diffusion time scales (compared to molecular mixtures), resulting in very small Lewis numbers of $L \approx 0.0001$ compared to $L = 0.01$–0.1 for molecular mixtures. It was also found that colloids often have a much stronger Soret effect, so that Ψ can be about 2 or 3 orders of magnitude larger than in binary mixtures [22]–[25]. Due to these much longer time scales and often a dramatic reduction in the threshold value, convection experiments in colloidal suspension are more difficult. A large Soret coefficient in macromolecular solutions and the resulting decrease of the convection threshold have already

been reported in 1977 [26, 27]. More recently, colloidal suspensions with large negative separation ratios have become popular for experimentally studying convection in the strongly supercritical regime, considering for example the evolution, distribution and stability of spatial structures [24, 25, 28] or the convective heat transfer [29]. Recent theoretical investigations have concentrated on developing convection for high Rayleigh numbers [30] and the peculiarities of the strongly distinct diffusion time scales [31, 32]. A survey of the patterns expected in the typical parameter range for colloidal suspensions can be found in [33].

In this paper, we report on convection experiments in a thermosensitive colloidal suspension. The core–shell particles used in this suspension have the intriguing feature that they change their size with temperature, which in turn leads to a strongly temperature-dependent viscosity. As a result, we expect a modified convection behaviour, especially for larger temperature differences. The remainder of the paper is organized as follows. The material characteristics of the suspension under consideration are described in detail in section 2.1, while the convection cell and the optical setup are explained in sections 2.2 and 2.3, respectively. In section 3.1, a qualitative comparison of the convection in our substance with convection in water is given. The experimental results for the threshold characteristics of the observed patterns are presented in section 3.2 and again compared with the results for water. The transient oscillation behaviour of the patterns when changing the temperature difference is presented qualitatively and quantitatively in section 3.3. In section 4, the various results of this paper, i.e. the reduction of the critical temperature difference, the wavelength of the convection patterns and the transient oscillations, are separately discussed and compared with the existing literature. Finally, a short outlook is given in section 4.4.

2. Description of the experiment

2.1. Material characteristics of the suspension

The thermosensitive colloidal suspension used in this experiment consists of core-shell nanoparticles in water. The particles have a solid polystyrene core and a grafted network of poly(*N*-isopropylacrylamide) (PNIPA), which changes its size with temperature. For low temperatures, the PNIPA network is swollen, which leads to the formation of hydrogen bonds between the water molecules and the amide side chains of the network. For higher temperatures, the PNIPA network undergoes a transition that leads to the expulsion of water molecules and results in a shrinking of the network [34]–[36]. This is shown schematically in the inset of figure 1(a).

The mass ratio of the components of the particles is $m_{\mathrm{PS}}/m_{\mathrm{PNIPA}} = 1.059 \pm 0.16$, where 'PS' stands for the polystyrene core and 'PNIPA' for the network. Details of the properties and of the synthesis of the particles can be found in [35, 37]. The radius $R_{\mathrm{c}} = 40.55\,\mathrm{nm}$ of the polystyrene core has been determined by directly imaging a frozen sample of particles with a Zeiss 922 transmission electron microscope [36], while the hydrodynamic radius of the whole particles has been determined by dynamic light scattering of a dilute suspension with a Peters ALV 800 goniometer [38]. As reported in [39], the hydrodynamic radius of the investigated particles can in good approximation be regarded as the average geometrical radius. As shown in figure 1(a), for temperatures below approximately 27 °C, R_{h} decreases almost linearly with rising temperatures, while it decreases much more dramatically when the PNIPA network is collapsed near the transition temperature of about 35 °C.

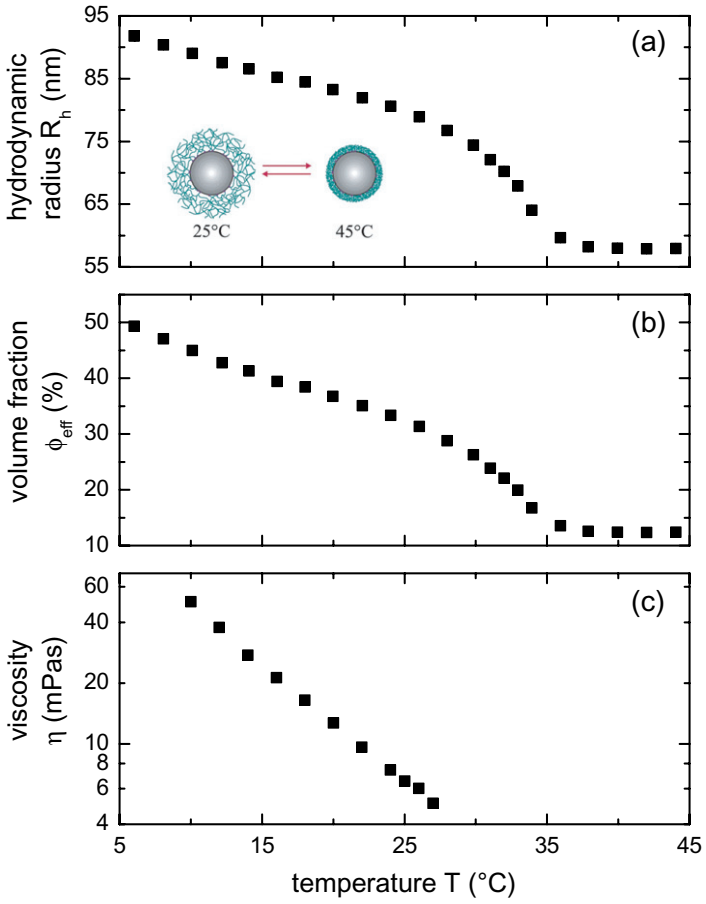

Figure 1. Illustration of the transition of the core-shell particles. For temperatures above ≈35 °C, the shell network is shrunken to its smallest size, while it swells for lower temperatures, leading to a larger hydrodynamic radius. Shown as functions of the temperature T are (a) the hydrodynamic radius R_h, (b) the resulting volume fraction ϕ_{eff} of the particles in the suspension and (c) the viscosity η of the suspension, respectively.

For our convection experiments, we use a suspension of particles in water with a mass concentration of $c = 8.71\%$. Using the values for the hydrodynamic radius R_h from figure 1(a) and the core radius R_c from above, the effective volume fraction ϕ_{eff} shown in figure 1(b) can be calculated as [40]

$$\phi_{eff} = \phi_c \left(\frac{R_h}{R_c}\right)^3. \tag{4}$$

Here,

$$\phi_c = \frac{V_c}{V} = c\,\frac{\rho_c}{\rho_{PS}}\,\frac{m_{PS}}{(m_{PS}+m_{PNIPA})} \tag{5}$$

represents the volume fraction of core material in the suspension, which is given by the density fraction $\rho_{PS}/\rho = 1.049 \pm 0.01$ of polystyrene and water, and the core-shell mass ratio m_{PS}/m_{PNIPA} [39].

Table 1. The material properties of the investigated colloidal suspension for a temperature of 25 °C. Reference values for water [43, 44] are given where applicable.

			Suspension	Water
Mass concentration	c	(%)	8.7 ± 0.2	–
Volume fraction	Φ		0.32 ± 0.05	–
Density	ρ	(10^3 kg m^{-3})	1.0053 ± 10^{-4}	$0.997\,047 \pm 10^{-6}$
Thermal expansion	α	(10^{-4} K^{-1})	2.9 ± 0.1	$2.572\,922 \pm 3 \times 10^{-6}$
Solutal expansion	β	(10^{-2} K^{-1})	9.38 ± 0.04	–
Dynamic viscosity	η	(10^{-3} Pa s)	6.6 ± 0.6	0.8900 ± 0.0015
	$\eta^{-1}\,\partial\eta/\partial T$	(K $^{-1}$)	-0.134 ± 0.002	$-0.022\,79$
	$\eta^{-1}\,\partial\eta/\partial c$		35 ± 3	–
Kinematic viscosity	ν	(10^{-6} m^2 s^{-1})	6.5 ± 0.6	0.893 ± 10^{-3}
	$\nu^{-1}\,\partial\nu/\partial T$	(K $^{-1}$)	-0.133 ± 0.002	$-0.022\,53$
	$\nu^{-1}\,\partial\nu/\partial c$		35 ± 3	–
Thermal diffusivity	κ	(10^{-7} m^2 s^{-1})	1.36 ± 0.05	1.46 ± 0.03
Mass diffusivity	D	(10^{-12} m^2 s^{-1})	6.79 ± 0.03	–
Soret coefficient	S_T		0.35 ± 0.03	–
Refractive index	n		$1.350\,7 \pm 2 \times 10^{-4}$	$1.331\,62 \pm 2 \times 10^{-5}$
(632.8 nm)	$\partial n/\partial T$	(10^{-4} K^{-1})	-1.3 ± 0.1	$-1.055\,090$
	$\partial n/\partial c$		0.23 ± 0.01	–
Prandtl number	$P = \nu/\kappa$		48	6.13 ± 0.02
Lewis number	$L = D/\kappa$		5.0×10^{-5}	–
Separation ratio	$\Psi = \frac{\beta}{\alpha} S_\mathrm{T} c(1-c)$		8.8	–

The viscosity of the suspension depends on the applied shear velocity [41, 42]. The dynamic viscosity is measured with an Anton Paar Physica MCR 301 rotational rheometer at different shear rates and extrapolated to low shear rates, in order to determine the zero-shear viscosity η [41]. The result is shown in figure 1(c).

The macroscopic material properties of the suspension are summarized in table 1 for a temperature of 25 °C. The density ρ is measured with an Anton Paar DMA4100 vibrating tube densitometer and the refractive index n with an automatic Abbe refractometer (Anton Paar AbbeMat WR, customized to a wavelength of 632.8 nm). Within the achievable accuracy, the density and refractive index were found to increase linearly with the mass concentration. The expansion coefficients $\alpha = -\rho^{-1}\,\partial\rho/\partial T$ and $\beta = \rho^{-1}\,\partial\rho/\partial c$ as well as the derivatives $\partial n/\partial T$ and $\partial n/\partial c$ are determined by fitting a polynomial of second order in the temperature and first order in the concentration to a series of measurements in the range of $T = 0 \ldots 30$ °C and $c = 0 \ldots 8.71\%$. The thermal diffusivity κ of the solution has not been measured, but has been estimated from the properties of the components using the Hashin–Strikman-bounds for the thermal conductivity and a mass weighted average of the heat capacities [45]. For our temperature range, the variation of κ determined with this method lies well within the bounds given in table 1. The collective mass diffusivity D and the Soret coefficient S_T are determined by a beam deflection technique as presented by [46, 47], using the convection cell described below but heating from the top to suppress convection. Here, the deflection of a laser beam by

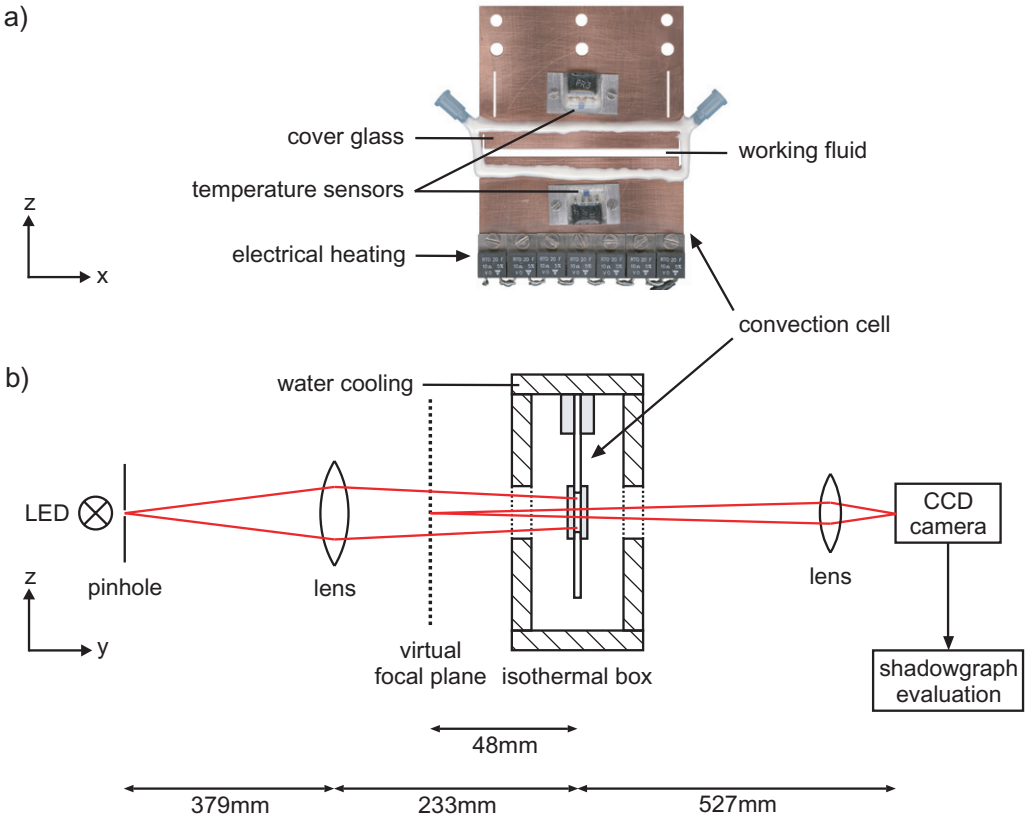

Figure 2. (a) Photograph of the convection cell. (b) Schematic diagram of the shadowgraph setup (not to scale).

the concentration gradient inside the cell allows a very sensitive measurement of the parameters in question. S_T is determined from the absolute value of the deflection, while D follows from the time constant of the measurement. Due to the long time scales of the experiment, we have done this for one temperature only, i.e. 25 °C.

2.2. *Convection cell*

Figure 2(a) is a photograph of the cell, that has been used for the convection experiments. In such a geometry, the convection flow is typically two-dimensional with the convection roll axes being aligned parallel to the shortest dimension (here the y-direction), and the flow is stable up to large supercritical Rayleigh numbers [48, 49].

The convection cell is made from a copper plate with the dimensions 70 mm × 90 mm × 1.5 mm. The convection channel has been cut out of the middle of the copper plate and has a length of $l = 68$ mm and a height of $d = (3.00 \pm 0.01)$ mm. The working fluid can be filled into the convection channel from left or right via two syringes which have a diameter of 0.6 mm each. The front and the back of the convection channel are sealed with glass plates. Due to the glue, the width b of the channel is somewhat larger than the thickness of the copper plate. We measured $b = (1.61 \pm 0.03)$ mm, leading to an aspect ratio of $\Gamma = d/b = 1.863 \pm 0.035$.

The temperatures at the bottom and top of the channel are measured by two platinum temperature sensors (JUMO Pt1000). Their resistances are measured by four-wire setups using

two digital multimeters (Prema 5017). The sensors are attached onto small aluminium discs that are screwed onto the convection cell. The distances of the two temperature sensors from the top and bottom of the channel are 15 mm, respectively. The heating of the bottom of the convection channel is done electrically by 14 power resistors (Vishay RTO20, 10 Ω each), which are connected in series. These resistors are mounted to the bottom of the copper plate. The heating voltage is provided by a power supply (EuroTest LAB/SL-30) and measured using a digital multimeter (Agilent 34410A/11A). Heat conductive paste has been applied to the back of the temperature sensors and the power resistors, respectively, to improve the thermal contact with the copper plate. The accuracy of the temperature difference was measured as ±10 mK. The thermal diffusion time for the convection cell was found to be approximately 5 min.

As seen in the middle part of figure 2(b), the convection cell is placed inside an isothermal aluminium box, which is kept at a constant temperature by a water circulation thermostat (Julabo F33-MW). The top of the convection cell is in thermal contact with this aluminium box. The bottom of the aluminium box is thermally insulated from the surrounding by a teflon plate. To further improve the thermal insulation, the box is inside another box made from polystyrene.

2.3. Optical setup

The convection channel can be illuminated from one side and observed from the other side through two slits at the front and at the back of the box. The shadowgraph method is used for observing the convection patterns [50, 51]. Figure 2(b) is a schematic drawing of the optical setup. An optical bench (Spindler and Hoyer) attached to a granite table is used for mounting the optical components. The point light source consists of an LED (Luxeon LED LXHL-LD3C; power 3 W, emission wavelength 627 nm) and a pinhole with a diameter of 0.2 mm. The current for the light source is provided by a power supply (EuroTest LAB/SL-30). A convex lense with a focal length $f_L = 250$ mm is used to illuminate the convection cell with slightly convergent light. The shadowgraph images are recorded with a monochrome USB2.0 CCD camera (Lumenera Lu135) with a macro objective (Micro-NIKKOR 55 mm $f/2.8$). The objective is focused onto the virtual focal plane. By using fine adjustment drives, all optical components can be moved in the x- and the z-direction.

3. Measurements and results

3.1. Qualitative comparison with convection in water

Figure 3 shows shadowgraph images of thermal convection in water (top) and in our thermosensitive colloidal suspension (bottom), respectively. The image for water was taken at a slightly supercritical temperature difference of $\Delta T = 11.46$ K, while the one for the suspension is shown for presentation purposes at a strongly supercritical temperature difference of $\Delta T = 3.17$ K. The bright vertical stripes correspond to upward streaming warmer fluid, while the darker regions or stripes in between correspond to downward streaming colder fluid. Two adjacent intensity maxima always separate a pair of counter-rotating convection rolls from the next pair.

One striking feature is the difference in wavelengths between the two images. Obviously, the wavelength observed in the suspension is significantly shorter than in water. While we probably measure a value close to the critical one in water, this is not the case for the suspension,

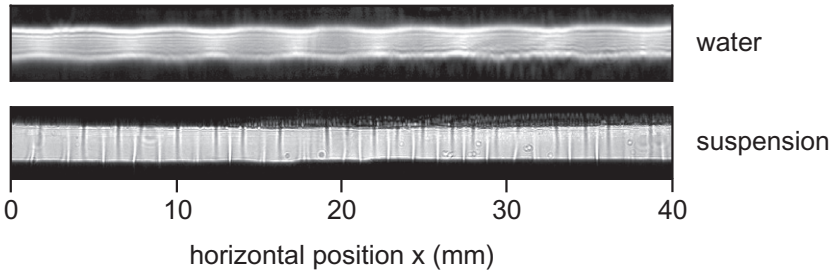

Figure 3. Shadowgraph images showing the thermal convection patterns in pure water (top) and in our thermosensitive colloidal suspension (bottom).

where the critical wavelength is expected to be of the order of the length of the convection channel. This will be discussed in more detail below and in section 4.

3.2. Determination of the threshold

In order to measure the convection threshold, the upper part of the convection cell was held at a constant temperature of about 25 °C by means of the water circulation thermostat, while the lower part was heated by applying a certain voltage to the electrical heating. The resulting temperature difference ΔT was measured by the temperature sensors and a shadowgraph image was recorded every minute. From each image, the optical contrast was extracted in the following way. First, the two-dimensional shadowgraph image is reduced to one line by adding up all horizontal lines spanning over the whole convection channel. To eliminate inhomogeneities of the illumination of the convection channel, the resulting line is divided by a zero line, which has been obtained in the same way but for a temperature difference of zero, i.e. without convection. This leads to a normalized intensity profile

$$I_{\mathrm{n}}(x) = \frac{\sum_{z_1}^{z_2} I(x,z)}{\sum_{z_1}^{z_2} I_0(x,z)}, \tag{6}$$

where z_1 and z_2 label horizontal lines, which are well inside the dark regions below and above the convection channel in figure 3. The optical contrast σ is obtained by calculating the rms value of such a line and dividing it by the mean intensity of the line:

$$\sigma = \frac{\mathrm{rms}(I_{\mathrm{n}})}{\bar{I}_{\mathrm{n}}} \tag{7}$$

with

$$\mathrm{rms}(f) = \sqrt{\frac{\sum_{x_1}^{x_2}(f(x)-\bar{f})^2}{(x_2-x_1+1)}} \quad \text{and} \quad \bar{f} = \frac{\sum_{x_1}^{x_2} f(x)}{(x_2-x_1+1)}. \tag{8}$$

When there is no convection in the channel, a contrast of $\sigma = 0$ is expected, while it should depart from 0 as soon as convection sets in. The result of such a measurement series is shown in figure 4, where the squared optical contrast σ^2 is plotted versus the applied temperature difference ΔT. Starting from a slightly negative value, the applied temperature difference was increased every 20 h by 0.103 K. For each data point, the optical contrast σ has been averaged over 5 h after a waiting time of 15 h.

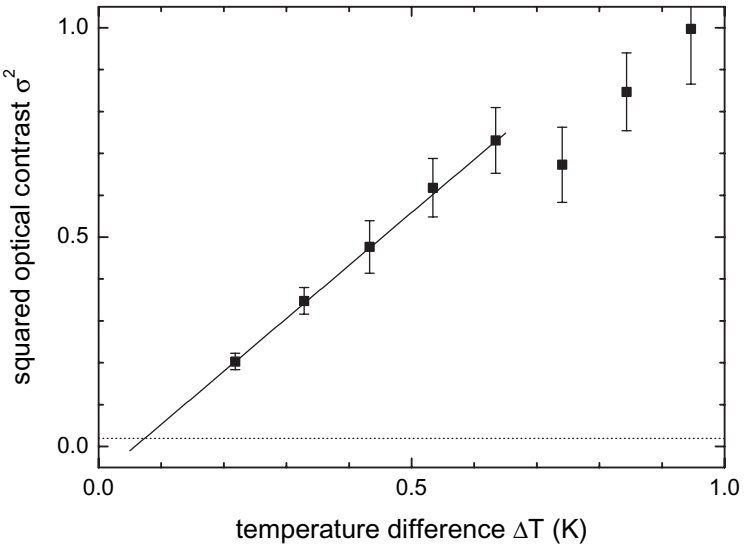

Figure 4. Squared optical contrast σ^2 of the shadowgraph patterns in the thermosensitive colloidal suspension as a function of the applied temperature difference ΔT. The dotted horizontal line denotes the noise level of the shadowgraph signals, while the solid line is a linear fit to the first five data points.

For $\Delta T < 0.2\,\mathrm{K}$, no data points are shown because no convergence of the contrast was found within the waiting time. This is not surprising, since in the vicinity of the convection threshold, the time scale for the onset is expected to be determined by the mass diffusion time $\tau_\mathrm{D} \approx 37\,\mathrm{h}$ and the relative distance from threshold, $\varepsilon = (R - R_\mathrm{c})/R_\mathrm{c}$.

The solid line is a linear fit of the first five data points, while the dotted line represents the noise level of the shadowgraph signals. If a pitchfork bifurcation is assumed for the instability, the critical temperature difference for the onset of thermal convection can be estimated from the intersection of the two lines as $\Delta T_\mathrm{c} \approx (0.07 \pm 0.03)\,\mathrm{K}$.

It should be noted that the observed pattern does not represent the critical wavelength, which is theoretically expected to be infinitely long or in our experiment of the order of the length of the convection channel. However, the neutral curve of the instability is essentially flat for our material parameters, so that the threshold for the observed wavelength is of the same order as for the critical one [19]–[21], [33]. In the measurement at $\Delta T \approx 0.7\,\mathrm{K}$, a change of the average wavelength from $\lambda = 0.75\,d$ to $\lambda = 0.66\,d$ was observed, resulting in a distinct change of the optical contrast. Therefore, the last three data points in figure 4 have been excluded from the evaluation.

For characterizing our apparatus, we performed a reference measurement of the convection onset in water. We measured a critical temperature difference of $\Delta T_\mathrm{c}^\mathrm{w} = (9.82 \pm 0.01)\,\mathrm{K}$, corresponding to a critical Rayleigh number of $R_\mathrm{c}^\mathrm{w} = 6630 \pm 150$ and a critical wavelength of $\lambda_\mathrm{c}^\mathrm{w} = (1.65 \pm 0.02)\,d$.

3.3. Transient oscillations

When changing the temperature difference, we observed a transient oscillation behaviour of the convection structures. Figure 5 shows a space–time plot of such a thermal convection

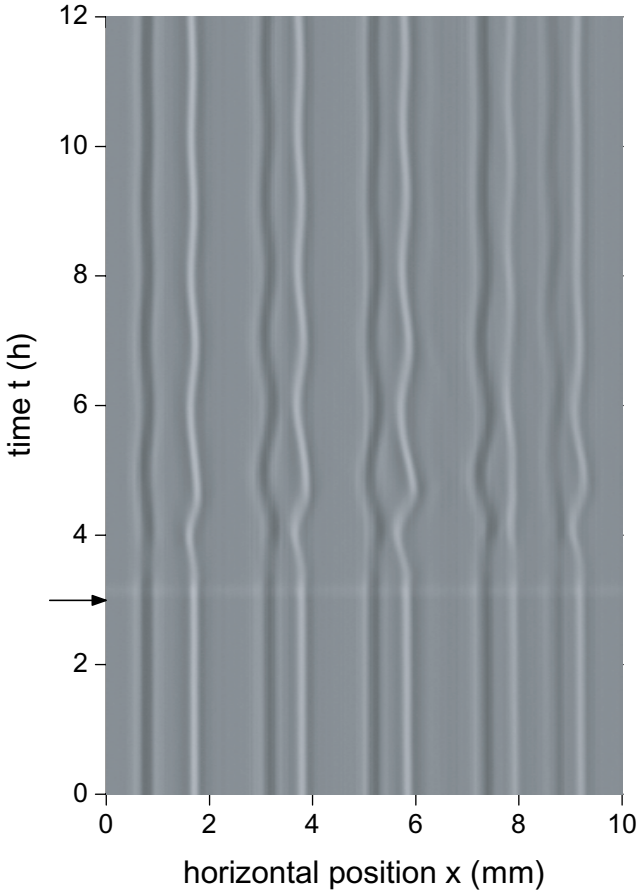

Figure 5. Space–time plot of shadowgraph images averaged over z. The temperature difference is held constant at $\Delta T = 1.47\,\mathrm{K}$, except that after 3 h (indicated by the arrow) it has been switched off for 10 min.

experiment. Each horizontal line of the image represents a normalized intensity profile $I_n(x)$, calculated according to equation (6) but scaled to maximum contrast for presentation purposes. The images were recorded in time steps of approximately one minute and the measurement is shown for 12 h. The bright spots correspond to the warmer upstreaming fluid, while the dark spots mark the colder downstreaming fluid. For the duration of the experiment, the temperature difference was held constant at $\Delta T = 1.47\,\mathrm{K}$, except that after 3 h it has been switched off for 10 min (indicated by the arrow). Before switching off ΔT, straight lines can be seen in figure 5, corresponding to a stationary convection pattern. After switching the temperature difference on again, the convection patterns exhibit spatial oscillations around their equilibrium positions. These oscillations slowly decay and vanish after approximately 9 h. Upstreaming and downstreaming flows oscillate against each other with the same frequency, which in this case is $f \approx 1.5\,\mathrm{mHz}$. A similar behaviour was found for other temperature differences as well.

Figure 6 shows the frequency f of the transient oscillations as a function of the temperature difference ΔT. The oscillation frequency f was determined by measuring the time τ of two consecutive oscillation maxima of one convection structure and then averaging over all such times extracted from one structure. After this has been done for all convection structures in one image, all individual times are averaged to obtain the oscillation frequency for this particular

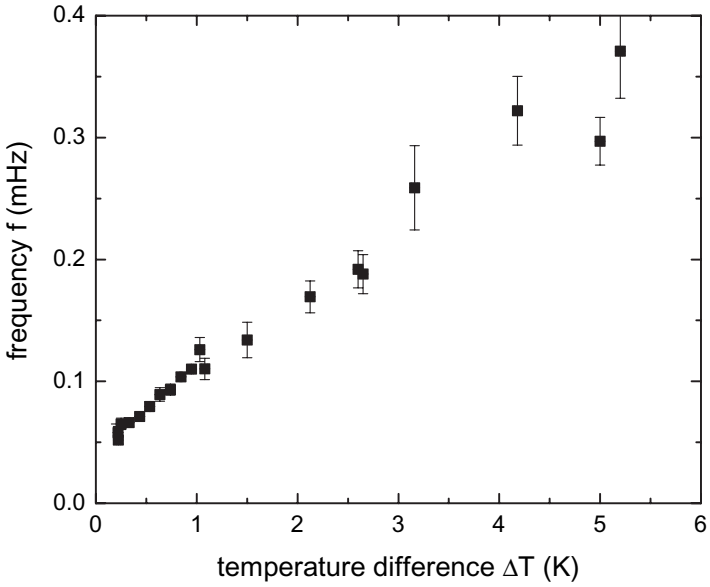

Figure 6. Frequency f of the transient oscillations as a function of the applied temperature difference ΔT.

temperature difference. The error bars in figure 6 simply represent the statistical errors coming from this procedure. Obviously, the transient oscillation frequency increases with increasing temperature difference.

4. Discussion and summary

4.1. Reduction of the critical temperature difference

For a pure fluid, the theoretical modeling of a laterally infinitely extended thin cell with perfectly heat conducting top and bottom boundaries and perfectly insulating front and back covers yields a critical Rayleigh number of $R_c = 3530 \pm 80$ and a critical wavelength of $\lambda_c = (1.963 \pm 0.001)\, d$ for our aspect ratio of $\Gamma = 1.86$ [52]. The complementary calculation for perfectly heat-conducting front and back covers predicts a convection onset at $R_c = 8130 \pm 100$ with a critical wavelength of $\lambda_c = (1.51 \pm 0.05)\, d$ [53]. For insulating covers, the critical wavelength shows only a weak dependence on the aspect ratio, while for conducting covers, it decreases noticeably with increasing aspect ratio. The top and bottom copper plates of our experimental cell may be regarded as perfectly heat conducting; however, the front and back glass plates have a thermal conductivity that is of the same order as for the liquid. Consequently, the observed critical Rayleigh number $R_c^w = 6630$ and critical wavelength $\lambda_c^w = 1.65\, d$ for the convection onset of water in our cell are found to lie between the two limiting cases.

Assuming a pure fluid ($\Psi = 0$) with otherwise the same material parameters as for our suspension, especially with the same viscosity, we find that the critical temperature difference would be about a factor of 5.9 larger than in water (see table 1 and equation (1)). From our reference measurements for water, we can thus deduct a hypothetical critical temperature difference of $\Delta T_c^{\Psi=0} \approx 58\,\mathrm{K}$ in our cell, so that our measurement for the suspension ($\Delta T_c \approx 0.07\,\mathrm{K}$) suggests a threshold reduction by a factor of at least 800.

A reduction of the threshold of convection in a suspension is expected when the material can be modelled as a binary fluid mixture with a positive separation ratio [14, 15]. Depending on the parameters of the suspension, this reduction can be quite dramatic as it is obviously the case in our experiment. This behaviour is reminiscent of former observations, which also showed a large threshold reduction, but for a negative separation ratio with heating from above [26, 27].

With the material parameters for our suspension ($\Psi = 8.8$ and $L = 0.000\,050$, see table 1), the theory for a thin convection cell with an aspect ratio of $\Gamma = 1.86$ yields $R_c = 0.0080$ and $\lambda_c = \infty$ [52]. Taking into account the correction deducted from the comparison of the experiment in water with the theory for perfectly insulating front and back covers, and assuming that this correction holds for our parameters as well, we can estimate $R_c \approx 0.015$. This translates into a critical temperature difference of $\Delta T_c \approx 0.000\,17$ K, which is much lower than the observed value of 0.07 K and also seems beyond the experimental resolution. Thus we have to conclude that for any positive temperature difference applied to the suspension in our experiment, convection is always present.

4.2. Wavelength of the convection patterns

For the convection wavelength, we find much shorter values as expected. According to the theory, the critical wavelength for Soret-driven convection should be of the order of the length of the convection channel, i.e. a single large convection roll is expected. As already discussed, however, the neutral curve for such material parameters is extremely flat, so that a very wide band of wavelengths have approximately the same critical temperature difference. But why do we reproducibly observe such small wavelengths as shown e.g. in figure 3 and not just random ones?

As we have qualitatively observed by a particle-tracking method, the convection first develops in narrow boundary layers near the top and bottom boundaries of the convection channel. As a consequence, the wavelength of the convection rolls is of the order of the height of these boundary layers. This feature has been discussed previously and occurs when the maximum of the developing concentration gradient at the boundaries reaches an unstable value [25]. A similar effect is also well known from convection in simple fluids with a strongly temperature-dependent viscosity [54]. When after some time the convection extends over the whole height of the channel, the wavelength remains the same since it is typically well inside the neutral curve, i.e. it is stable. The lateral phase diffusion time is much too large for the critical wavelength to supersede the current one. Also in the well supercritical regime, as observed in our experiment, the wavelength remains essentially the same.

4.3. Transient oscillations

The mechanism of the observed transient oscillations of the convection pattern remains unclear. For the moment, we will restrict the discussion to a comparison with other published observations of oscillatory convection patterns. In simple fluids, several time-dependent patterns are known that appear as secondary instabilities for higher Rayleigh numbers before the transition to turbulent flow, both in bulk [11, 55] and in Hele–Shaw geometries [49, 56]. The observed inversely phased oscillation of the up and downstreams qualitatively resembles the behaviour of a standing oscillatory blob instability [57] or the spatial time evolution of the temperature field in thin slots [58, 59]. Further, the existence of an oscillatory instability

has been verified in viscoelastic suspensions with large viscosities and large viscoelastic relaxation times [60]. Since the gel fraction of our suspension is viscoelastic, some viscoelastic behaviour can be expected in sufficiently concentrated solutions of gel particles. Rheological measurements of the suspension indicate viscoelastic time scales of up to 1000 s, which is of the same order as the turn-over times of the convection rolls as well as the oscillation periods discussed here. In this frequency regime, however, the elastic properties are so weak that they are near the resolution limit of the rheometer (Anton Paar Physica MCR 301).

In nearly critical ^{3}He, employed as an example for a compressible fluid, a transient oscillatory heat transfer during the onset of convection was found [61]. A similar behaviour can be observed in measurements of the convection onset in materials with a very strong temperature-dependent viscosity [62]. Transient oscillations in the amplitude of Soret-driven convection after applying a temperature step have first been observed in a suspension with a large negative separation ratio heated from above [26, 27]. The same behaviour has also been reported for a molecular fluid mixture [63], for colloidal suspensions [24, 25] and in simulations [64]. (This supercritical transient oscillation mode must not be confused with the well-known oscillatory instability of a binary fluid mixture with negative separation ratio heated from below [14, 15].)

Both stationary and transient oscillations have been attributed to the repeated formation and remixing of thermal or concentration boundary layers, respectively [54, 65]. This also explains the noticeably short oscillation period in the Soret-driven case, since the time scale is determined by the smaller boundary layer height δ rather than by the cell height d. For the case of a simple fluid, the scaling behaviour for the typical time corresponding to this mechanism has been estimated [54, 66]. Using the diffusive propagation of the boundary layer height $\delta \propto t^{1/2}$ and the scaling of the Rayleigh number $R \propto \delta^3$, a dependency of $t \propto R^{-2/3}$ was derived, which has been confirmed by measurements of oscillating convection in simple fluids [54, 67]. In Hele–Shaw geometries, the scaling of the Rayleigh number has to be adjusted to the aspect ratio δ/b of the boundary layer to the cell thickness [56].

Figure 7 shows the oscillation period of the transient oscillations observed in our experiment in dimensionless form. The solutal Rayleigh number has been calculated according to equation (3) from the material parameters at the average cell temperature. The oscillation period $T_{\mathrm{osc}} = 1/f$ has been scaled with the mass diffusion time τ_{D}. From an (error weighted) least squares fit to the data, we obtain the scaling relation $T_{\mathrm{osc}}/\tau_{\mathrm{D}} \propto R_{\mathrm{s}}^{-0.52\pm0.03}$. The exponent differs significantly from the scaling discussed above for the simple fluid case but corresponds well to the dependencies that were found for the above-mentioned transient oscillations in ^{3}He and in Soret-driven convection [61, 68, 69].

4.4. Outlook

The dramatic decrease of the threshold value as predicted by the theory (a factor of about 400 000) together with the prohibitively large time scales involved limit the experimentally accessible temperature range to very large values of the (solutal) Rayleigh number. While this provides an opportunity to investigate a remarkably overcritical regime, it would be desirable to measure the convection onset with the same accuracy as used from other convection experiments. In order to improve the situation, we are currently designing a smaller setup with cell heights of $d \leqslant 1$ mm, resulting in an increase of the critical temperature difference and a reduction of the diffusion times by at least an order of magnitude. Moreover, measurements

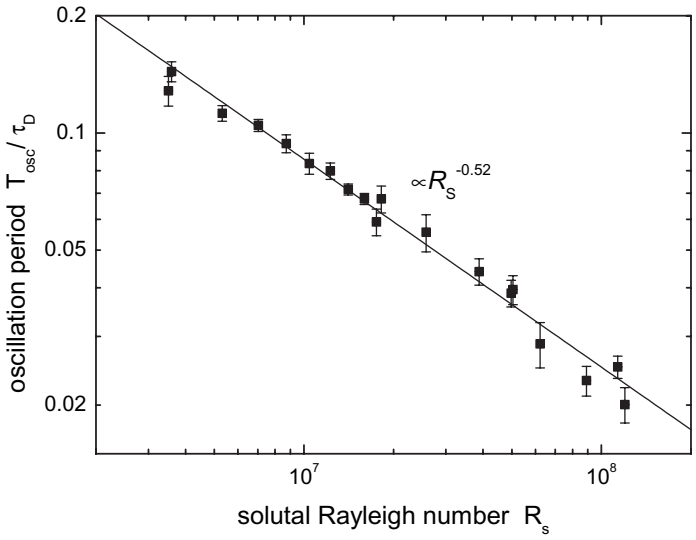

Figure 7. Dimensionless oscillation period T_{osc} of the transient oscillations as a function of the solutal Rayleigh number R_{s}. The line is a fit of a power law to the data.

with higher precision are planned for the Soret coefficient and for the mass diffusivity in our suspension. In order to explain the transient oscillations theoretically, we think that a complete nonlinear model of the colloidal suspension in a two-dimensional geometry is the most promising route.

Acknowledgments

We thank W Köhler and A Königer for providing the equipment and know-how for high-precision measurements of the refractive indices and FH Busse, M Gläßl, J Schmied and W Zimmermann for fruitful discussions. We gratefully acknowledge the financial support of the Deutsche Forschungsgemeinschaft (DFG) through the Forschergruppe FOR608, project 'Convection in Suspensions'.

References

[1] Ostwald C W W 1912 *Grundriss der Kolloidchemie* (Dresden: T Steinkopff)
[2] Myers D 1999 *Surfaces, Interfaces, and Colloids* 2 edn (New York: Wiley)
[3] Morrison I D 2002 *Colloidal Dispersions* (New York: Wiley)
[4] Ludwig C 1856 Diffusion zwischen ungleich erwärmten Orten gleich zusammengesetzter Lösungen *Sitzungsber. Akad. Wiss. Wien, Math.-Naturwiss. Kl.* **20** 539
[5] Soret M C 1879 Une dissolution saline primitivement homogène *Arch. Sci. Phys. Nat.* **3** 48–61
[6] Koonin E V 2007 An RNA-making reactor for the origin of life *Proc. Natl Acad. Sci. USA* **104** 9105
[7] Baaske P, Weinert F M, Duhr S, Lemke K H, Russell M J and Braun D 2007 Extreme accumulation of nucleotides in simulated hydrothermal pore systems *Proc. Natl Acad. Sci. USA* **104** 9346
[8] Chandrasekhar S 1961 *Hydrodynamic and Hydromagnetic Stability* (London: Oxford University Press)
[9] Landau L D and Lifschitz E M 1981 *Lehrbuch der Theoretischen Physik IV: Hydrodynamik* (Berlin: Akademie Verlag)

[10] Busse F H and Whitehead J A 1971 Instabilities of convection rolls in a high Prandtl number fluid *J. Fluid Mech.* **47** 305
[11] Busse F H 1978 Non-linear properties of thermal convection *Rep. Prog. Phys.* **41** 1929–67
[12] Cross M C and Hohenberg P C 1993 Pattern formation outside equilibrium *Rev. Mod. Phys.* **65** 851
[13] Bodenschatz E, Pesch W and Ahlers G 2000 Recent developments in Rayleigh–Bénard convection *Annu. Rev. Fluid Mech.* **32** 709
[14] Gershuni G Z and Zhukhovitskii E M 1976 *Convective Stability of Incompressible Fluids* (Jerusalem: Keter Publications)
[15] Platten J K and Legros J C 1984 *Convection in Liquids* (Berlin: Springer)
[16] Turner J S 1973 *Buoyancy Effects in Fluids* (Cambridge: Cambridge University Press)
[17] Lücke M, Barten W, Büchel P, Fütterer C, Hollinger S and Jung C 1998 Pattern formation in binary fluid convection and in systems with throughflow *Evolutions of Spontaneous Structures in Continuous Systems Lecture Notes in Physics* vol 55 ed F H Busse and S C Müller (Berlin: Springer) p 127
[18] Velarde M G and Schechter R S 1972 Thermal diffusion and convective stability. II. An analysis of the convected fluxes *Phys. Fluids* **15** 1707–14
[19] Knobloch E and Moore D R 1988 Linear stability of experimental Soret convection *Phys. Rev.* A **37** 860–70
[20] Cross M C and Kim K 1988 Linear instability and the codimension-2 region in binary fluid convection between rigid impermeable boundaries *Phys. Rev.* A **37** 3909–20
[21] Schöpf W and Zimmermann W 1993 Convection in binary fluids - amplitude equations, codimension-2 bifurcation, and thermal fluctuations *Phys. Rev.* E **47** 1739–64
[22] Wiegand S 2004 Thermal diffusion in liquid mixtures and polymer solutions *J. Phys.: Condens. Matter* **16** R357–79
[23] Piazza R and Parola A 2008 Thermophoresis in colloidal suspensions *J. Phys.: Condens. Matter* **20** 153102
[24] Cerbino R, Vailati A and Giglio M 2002 Soret driven convection in a colloidal solution heated from above at very large solutal rayleigh number *Phys. Rev.* E **66** 055301
[25] Cerbino R, Mazzoni S, Vailati A and Giglio M 2005 Scaling behavior for the onset of convection in a colloidal suspension *Phys. Rev. Lett.* **94** 064501
[26] Giglio M and Vendramini A 1977 Soret-type motion of macromolecules in solution *Phys. Rev. Lett.* **38** 26–30
[27] Giglio M and Vendramini A 1977 Buoyancy-driven instability in a dilute solution of macromolecules *Phys. Rev. Lett.* **39** 1014–7
[28] Giavazzi F and Vailati A 1975 Scaling of the spatial power spectrum of excitations at the onset of solutal convection in a nanofluid far from equilibrium *Phys. Rev. Lett.* **34** 561–4
[29] Donzelli G, Cerbino R and Vailati A 2009 Bistable heat transfer in a nanofluid *Phys. Rev. Lett.* **102** 104503
[30] Kim M C, Hong J S and Choi C K 2006 The analysis of the onset of Soret-driven convection in nanoparticles suspensions *AIChE J.* **52** 2333–9
[31] Ryskin A, Müller H W and Pleiner H 2003 Thermal convection in binary fluid mixtures with a weak concentration diffusivity, but strong solutal buoyancy forces *Phys. Rev.* E **67** 046302
[32] Shliomis M I and Smorodin B L 2005 Onset of convection in colloids stratified by gravity *Phys. Rev.* E **71** 036312
[33] Huke B, Pleiner H and Lücke M 2002 Convection patterns in colloidal solutions *Phys. Rev.* E **75** 036203
[34] Shibayama M, Tanaka T and Han C C 1992 Small-angle neutron-scattering study on poly(*N*-isopropylacrylamide) gels near their volume-phase transition-temperature *J. Chem. Phys.* **97** 6829–41
[35] Ballauff M and Lu Y 2007 'Smart' nanoparticles: preparation, characterization and applications *Polym.* **48** 1815–23
[36] Crassous J J, Wittemann A, Siebenbürger M, Schrinner M, Drechsler M and Ballauff M 2008 Direct imaging of temperature-sensitive core-shell latexes by cryogenic transmission electron microscopy *Coll. Polym. Sci.* **286** 805–12

[37] Dingenouts N, Norhausen C and Ballauff M 1998 Observation of the volume transition in thermosensitive micronetworks by small-angle x-ray scattering *Macromolecules* **31** 8912–7
[38] Berne B J and Pecora R 2000 *Dynamic Light Scattering* (New York: Dover)
[39] Crassous J J, Siebenbürger M, Ballauff M, Drechsler M, Henrich O and Fuchs M 2006 Thermosensitive core-shell particles as model systems for studying the flow behavior of concentrated colloidal dispersions *J. Chem. Phys.* **125** 204906
[40] Crassous J J, Ballauff M, Drechsler M, Schmidt J and Talmon Y 2006 Imaging the volume transition in thermosensitive core-shell particles by cryo-transmission electron microscopy *Langmuir* **22** 2403–6
[41] Senff H, Richtering W, Norhausen C, Weiss A and Ballauff M 1999 Rheology of a temperature sensitive core-shell latex *Langmuir* **15** 102–6
[42] Deike I and Ballauff M 2001 Rheology of thermosensitive latex particles including the high-frequency limit *J. Rheol.* **45** 709–20
[43] The International Association for the Properties of Water and Steam 1997 Release on the refractive index of ordinary water substance as a function of wavelength, temperature and pressure. http://www.iapws.org
[44] The International Association for the Properties of Water and Steam 2008 Supplementary release on properties of liquid water at 0.1 MPa http://www.iapws.org
[45] Milton G W 1981 Concerning bounds on the transport and mechanical properties of multicomponent composite materials *Appl. Phys.* A **26** 125–30
[46] Zhang K J, Briggs M E, Gammon R W and Sengers J V 1996 Optical measurement of the Soret coefficient and the diffusion coefficient of liquid mixtures *J. Chem. Phys.* **104** 6881–92
[47] Giglio M and Vendramini A 1975 Thermal-diffusion measurements near a consolute critical point *Phys. Rev. Lett.* **34** 561–4
[48] Hartline B K and Lister C R B 1977 Thermal convection in a Hele–Shaw cell *J. Fluid Mech.* **79** 379–89
[49] Kvernold O 1979 On the stability of non-linear convection in a Hele–Shaw cell *Int. J. Heat Mass Transfer* **22** 395
[50] Eichler H-J *et al* 1993 *Bergmann, Schäfer/Lehrbuch der Experimentalphysik/Band 3—Optik* (Berlin: Walter de Gruyter)
[51] Rasenat S, Hartung G, Winkler B L and Rehberg I 1989 The shadowgraph method in convection experiments *Exp. Fluids* **7** 412
[52] Schöpf W 1992 Convection onset for a binary mixture in a porous-medium and in a narrow cell—a comparison *J. Fluid Mech.* **245** 263–78
[53] Frick H and Clever R M 1982 The influence of side walls on finite-amplitude convection in a layer heated from below *J. Fluid Mech.* **114** 467
[54] Busse F H 1989 Fundamentals of thermal convection *Mantle Convection, Plate Tectonics and Global Dynamics* ed W R Peltier (London: Gordon and Breach) pp 23–95
[55] Busse F H and Clever R M 1979 Instabilities of convection rolls in a fluid of moderate Prandtl number *J. Fluid Mech.* **91** 319–35
[56] Koster J N and Müller U 1982 Free convection in vertical gaps *J. Fluid Mech.* **125** 429–51
[57] Clever R M and Busse F H 1995 Standing and travelling oscillatory blob convection *J. Fluid Mech.* **297** 255–73
[58] Frick H and Müller U 1983 Oscillatory Hele–Shaw convection *J. Fluid Mech.* **126** 521–32
[59] Koster J N and Müller U 1984 Oscillatory convection in vertical slots. *J. Fluid Mech.* **139** 363–90
[60] Kolodner P 1998 Oscillatory convection in viscoelastic DNA suspensions *J. Non-Newtonian Fluid Mech.* **75** 167–92
[61] Kogan A B and Meyer H 2001 Heat transfer and convection on set in a compressible fluid: ^{3}He near the critical point *Phys. Rev.* E **63** 056310
[62] Davaille A and Jaupart C 1993 Transient high-Rayleigh-number thermal convection with large viscosity variations *J. Fluid Mech.* **253** 141–66

[63] La Porta A and Surko C M 1998 Convective instability in a fluid mixture heated from above *Phys. Rev. Lett.* **80** 3759–62

[64] Ryskin A and Pleiner H 2005 Thermal convection in colloidal suspensions with negative separation ratio *Phys. Rev.* E **71** 056303

[65] Shliomis M I and Souhar M 2000 Self-oscillatory convection caused by the Soret effect *Europhys. Lett.* **49** 55–61

[66] Howard L N 1964 Convection at high Rayleigh number *Proc. 11th Int. Congress of Applied Mechanics* ed H Görtler (Berlin: Springer) pp 1109–15

[67] Martinet B and Adrian R J 1988 Rayleigh–Bénard convection: experimental study of time-dependent instabilities *Exp. Fluids* **6** 316–22

[68] Mazzoni S, Cerbino R, Brogioli D, Vailati A and Giglio M 2004 Transient oscillations in Soret-driven convection in a colloidal suspension *Eur. Phys. J.* E **15** 305–9

[69] Furukawa A, Meyer H, Onuki A and Kogan A B 2003 Convection in a very compressible fluid: comparison of simulations with experiments *Phys. Rev.* E **68** 056309